LINarm++
Affordable and Advanced LINear device for ARM rehabilitation

Deliverable D3.1
Mechatronic device design

Contractual delivery date	31.10.2015 (month 6)
Actual delivery date	31.10.2015 (month 6)
Version	1.0
Dissemination level	CO
Authors	Matteo Malosio (CNR) Giulio Spagnuolo (CNR) Marco Caimmi (CNR) Tito Dinon (CNR)

Table of Contents

Executive summary

This document is intended to present the redesigned version of LINarm, namely LINarm2.
Starting from experiments and preliminary clinical results performed with a more complex robotic devices (Chapter 1) the set of technical and functional requirements to be fulfilled by the redesigned version of LINarm2 are presented (Chapter 2).
The new device is characterized by a new Variable Stiffness Action, described in Chapter 3.
The detailed mehanical design is presented in Chapter 4.
Electrical components and their connections are described in Chapter 5.

1 Introduction

1.1 Background

The upper limb is an incredible adaptive organ that allows performing high-level interactive movements and is capable of accomplishing numerous functional tasks in an infinitive number of kinematic solutions. It is a sophisticated multi-joint system designed for multitasking functioning and capable of performing from heavy jobs to tasks requiring fine movements, not to mention exploration and manipulation of objects [1]. Certainly, not all movements may be trained and this variability makes the selection of a reduced number of them necessary, a selection that, preferably, should be done on the basis of key determinants of the movement control.

In this framework of reasoning, an analysis of which are the main functions of the different joints/organs of the upper limb is helpful for finding a solution to the problem. Making a strong simplification, the shoulder may be seen as the joint that enables the orienteering in the space of the entire upper limb, the elbow as the elongation-shortening element that allows reaching objects (and taking them towards the body) and, finally, the hand as the end effector, the organ that enables direct interaction with the environment [2]. Within this schematic model, shoulder and elbow movements are propaedeutic for hand positioning in space and, therefore, the motor recovery of specific functional movements of these two joints becomes a primary issue in rehabilitation.

Given all this above, two functional gestures only are sufficient to study the shoulder and elbow compound movements that are frequently used in Activities of Daily Living (ADLs): 1) the Reaching Movement (RM, Fig. 1) against gravity and 2) the Hand-to-Mouth Movement (HtMM, Fig. 2) [3]. In fact, these particular gestures allow us to perform tasks like eating, reaching for objects and, taking them towards the body/face. Similarly, passing from assessment to rehabilitation, by training these two gestures only, motor recovery can be obtained of important compound movements like shoulder flexion (against gravity) and elbow extension, and, elbow flexion (against gravity) and shoulder flexion [4].

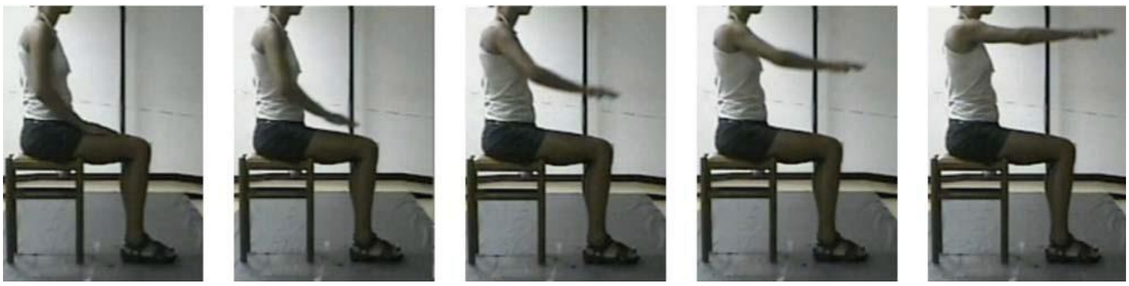

Fig. 1: Frame sequence of the Reaching Movement (RM) performed by a healthy subject.

Fig. 2: Frame sequence of the Hand to Mouth Movement (HtMM) performed by a healthy subject.

1.2 Preliminary results

A robotic rehabilitation protocol based on RM and HtMM was tested on 8 chronic stroke subjects [4] (the number of subjects is today 14).

The control of an industrial robot, a Mitsubishi Pa10, and the control graphic interface were customized for rehabilitation purposes following the requirements of the study. In Fig. 3, the robot is represented during RM and HtMM.

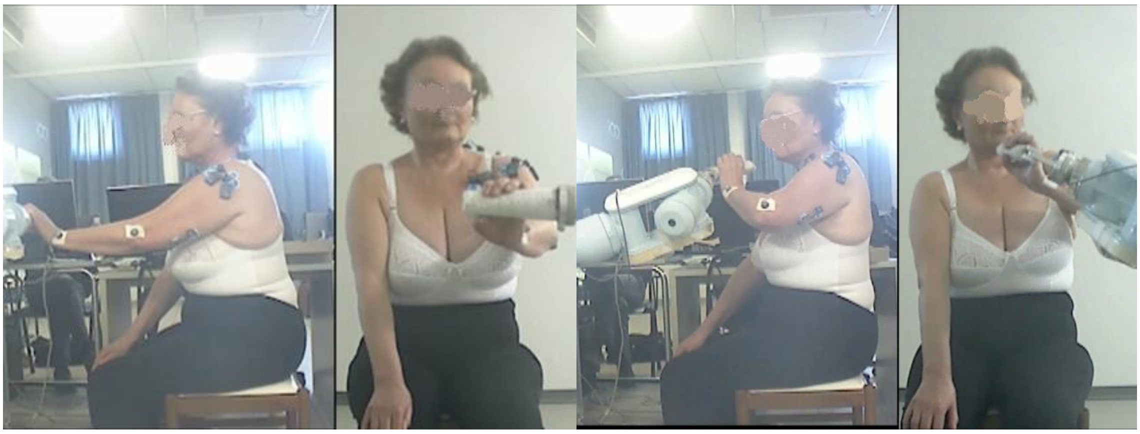

Fig. 3: Robot assisted Reaching Movement (left) and Hand-to-Mouth-Movement (right).
For HtMM the handle is articulated and can freely rotate through a passive universal joint.

The intervention consisted of 12 sessions. Every session consisted of 20 minutes of execution of RM against gravity and 20 minutes of HtMM. Velocities were rigidly imposed and were for both movements characterized by a bell-shaped velocity profile. Every minute the velocity was scaled with peak velocities comprised between 0.30 and 0.80 m/s (slow movements were alternated to the ones performed at physiological velocity, customizing the parameters on the patient's capability). During the mobilization, the patient was asked to alternately relax or to try to actively follow the rigidly imposed movement.

Synthetic results are reported in Fig. 4. Interestingly, general improvements were not correlated to time distance from the stroke event. Even more interestingly, almost all patients referred improvements at wrist and hand although the intervention was intended for shoulder and elbow functional recovery only. These results are extremely positive considering the short time of intervention (1 month) and the time of distance from the stroke (32±25 months).

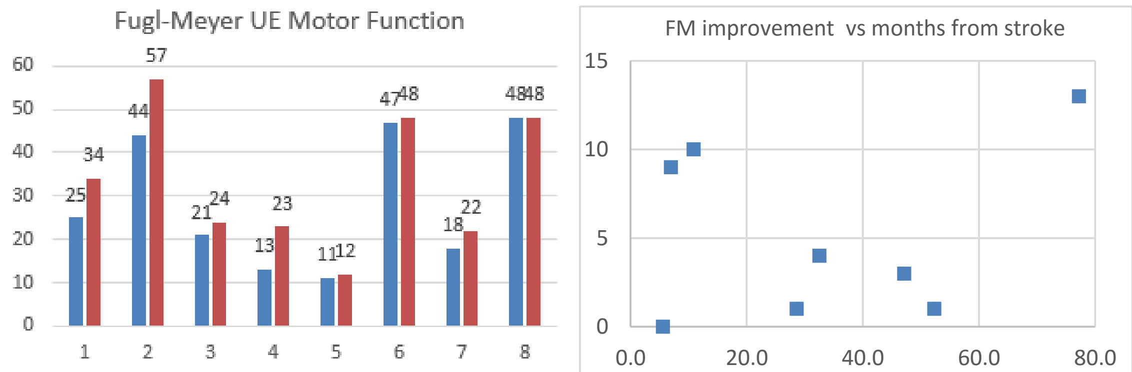

Fig. 4: Left: FM of each patient pre-intervention (blue) and post-intervention (red).
Right: FM improvement of each patient vs months from stroke event.

The results of the study are consistent with the literature and today recommendations in stroke rehabilitation which promote the use of trainings based on functional movements in general, on reaching in particular. In fact, retraining reach and grasp skills is critical for return to a full quality-of-life [5]. In the field of robotic rehabilitation, task-oriented training is emerging as the dominant and most effective approach to motor rehabilitation of the upper-limb function after stroke. Future robots for rehabilitation need to be task-oriented [6].

2 Requirements

2.1 Functional requirements

Considering the relevance of RM and HtMM and promising results obtained so far, a solution to enable patients to be trained by a robotic device with one these two movements is considered beneficial and constituted the origin of the LINarm device development.

With regard to the RM, the solution to the problem may be easily found in a simple support able to fix a linear axis to a table and enabling the possibility to incline it vertically (and horizontally) (Fig. 5). More complicated is the solution for the HtMM since the hand trajectory is not properly straight and, further considering that the movement is towards the face, the orientation of LINarm has to be accurately studied and the solution should be thought considering the also the use of properly customized handle (Fig. 6). Anyway, in both cases a linear movement represents a good approximation and, for this reason, the concept behind the LINarm device is considered promising.

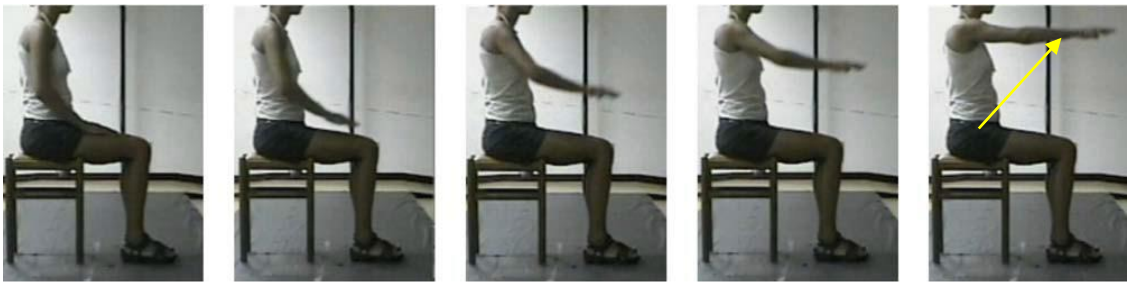

Fig. 5: The trajectory of the RM may be approximated to a straight one.

Fig. 6: The trajectory of the HtMM may be approximated to a straight one if special articulated handles are used.

For these reasons, the development of a modular solution enabling differently oriented movements, approximating them as linear, is considered a good compromise and strategy to be included in a low-cost device for home rehabilitation. Therefore, during the (re)design phase of LINarm this requirement must effectively by taken into account.

2.2 Technical requirements

Following indications reported in Deliverable *D1.1 - Requirements and specifications* and according to activities and experinces carried out so far exploiting the first version of LINarm [7], the following design guidelines have been drawn.

- Keep the Variable Stiffness Actuation concept but develop/apply a more compact and more effective VSA scheme (Chapter 3).
- Reduce the overall dimensions/weight of LINarm2 w.r.t. LINarm1 and simplify assembly operations in order to simplify installation procedures and reduce the encumbrance of mechanical components during the actual exploitation (Chapter 4.1.2).
- Move both antagonist motors at one side of the device to reduce the dimensions of the other side, to facilitate the execution of HtMM tasks and to optimize the position of the center of mass w.r.t. the support (Chapter 4.4).
- Foresee an orientable support to perform both RM and HtMM movements along different orientations (Chapter 2.1, Chapter 4.4).
- Fulfill safety requirements according to international norms (Chapter 0)
- Allow the installation of a sensorized handle to acquire physiological data (*Deliverable D4.1 - Proof-of-concept system for principles of user state assessment and design of sensory system*) and implement multi-òlvel patient-in-the-loop control algorithms (*Deliverable D2.1 - Control system architecture and components*).

3 Cam-based Variable Stiffness Actuation

3.1 Introduction

Variable Stiffness Actuators (VSA) allow the adjustment, in a controlled manner, of their own mechanical stiffness. A VSA is typically made up of two Series Elastic Actuators (SEA) arranged in parallel w.r.t. a mobile mass (Fig. 7). A SEA is, in general terms, made up of a rigid actuator and an elastic element (e.g. a spring) arranged serially. Two SEA featuring non-linear stiffness, arranged in parallel and exerting opposite forces, characterize a typical VSA. SEA stiffness nonlinearity is required to make the VSA stiffness adjustable [8].

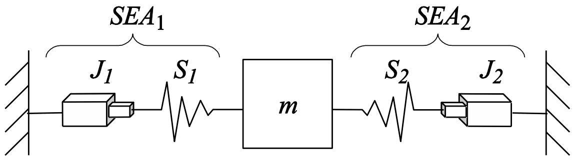

Fig. 7: The *antagonist configuration* of the *LWWCVSA* enabling a linear actuator to feature a variable stiffness behaviour: two non-linear SEA arranged in parallel allows to control the position and the stiffness of a mobile mass *m*.

The use of VSA, already adopted in different applications not requiring high positioning precision, can lead to the following features, considered really important for rehabilitation devices:

- *adjustable stiffness* requiring neither force sensors nor transmission backdrivability;
- *force estimation* by position sensors (e.g. potentiometers), typically cheaper than force sensors, being known the spring characteristic;
- suitability for a *direct interaction with human beings* since intrinsic mechanical compliance avoids high impulsive forces in case of malfunctioning or undesired movements.

Currently existing VSAs allow to feature a rotational actuator with a variable stiffness characteristic. In order to realize a linear axis featuring a variable stiffness actuator may be possible, therefore, to transmit the rotational motion of a rotational VSA to a carriage, by a belt-based or a wire-based transmission mechanism. The main limitation of this approach is that the vast majority of the so-far developed VSA allows to perform a limited rotational stroke, typically less than a round angle, except [9], preventing the realization of a long-stroke, theoretically unlimited, linear motion. On the other side, to author's knowledge, no VSA have been so far specifically developed for linear motions, required to realize the variable-stiffness motion of LINarm. The first version of LINarm has been realized exploiting a non-linear spring realized by a set of commercially available tension spring [7]. The solution allows to obtained a VSA characteristic but has drawbacks from the dimensions and stiffness-tuning point of view. To face these drawbacks the LWWC-VSA (i.e. Linear Wire-Wrapped Cam VSA) (Fig. 8) has been specifically conceived and developed. Moreover, its layout has been conceived with the specific objectives of realizing a system characterized by a limited number of components, a relatively clean and customizable design, characterized by a stress distribution which allows it to be realized by a common desktop 3d-printer, featuring also low-cost applications with a variable stiffness.

Fig. 8: Concept design of the Linear Wire-Wrapped Cam VSA (LWWC-VSA).

The LWWC-VSA features two antagonist LWWC-SEA (Linear Wire-Wrapped Cam – Series Elastic Actuator) configured in parallel, enabling to control both the eqilibrium position and the stiffness of a linear axis. In the following sections the actuator is presented, starting from the elements and the layout of a single LWWC-SEA, up to the configuration of the LWWC-VSA.

3.2 Linear Wire-Wrapped Cam – Series Elastic Actuator (LWWC-SEA)

As previously mentioned, the LWWC-VSA is made up of two antagonistic LWWC-SEA, each of them featuring a tunable stiffness characteristic. Its essential elements are a torsional spring, a cam and a wire, which properly configured allows to realize a linear spring characterized by a customizable non-linear stiffness characteristic.

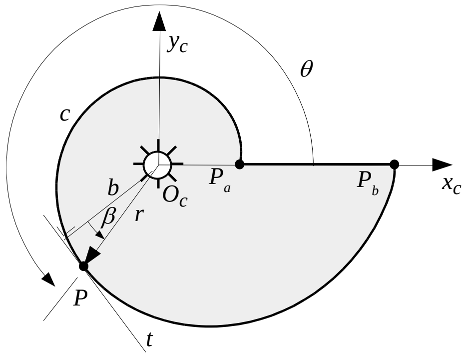

Fig. 9: Cam profile.

Let us denote by $\{f\}$ a generic planar reference frame, centered in O_f and defined by the orthogonal axes x_f and y_f.

Let us consider a cam defined by the curve c defined by the polar coordinates r and θ w.r.t. $\{c\}$ (Fig. 9). The cam is shaped as a spiral, for which r is a monotonic continuous function of θ. Let us denote by P generic point on the cam profile, by P_a and P_b the points of the cam profile characterized by the minimum and maximum value of r, respectively. Therefore, it is $\theta_a <= \theta <= \theta_b$. Let us denote by s the curvilinear coordinate of the cam segment $P_a \rightarrow P$. It is worth to recall that the curvilinear length of a curve segment expressed in polar coordinates between two points P_a and P_b is

$$s = \int_{P_a}^{P_b} \mathrm{d}s = \int_{P_a}^{P_b} \sqrt{r^2 + r_\theta^2}\, \mathrm{d}\theta$$

where [10]

$$r_\theta = \mathrm{d}r / \mathrm{d}\theta.$$

The pitch angle of the spiral profile is denoted by

$$\beta = \arctan\left(\frac{1}{r}\frac{\mathrm{d}r}{\mathrm{d}\theta}\right)$$

complement of the angle between the tangent and radial line [11].

The minimum distance of the tangent line to the center of the cam is

$$b = \frac{r}{\cos\beta}$$

Referring to Fig. 10 let us consider a revolute joint J_c constraining O_c to O_o, where O_o is the center of a reference frame $\{o\}$, so that $\{c\}$, and hence c, can rotate about O_o. The rotation angle of $\{c\}$ w.r.t. $\{o\}$ is denoted by γ. Let us consider that J_c is characterized by a torsional stiffness k_t which restraints the free rotation of c about O_o, by a reaction torque

$$\tau_t(\gamma) = \int_\gamma k_t\, \mathrm{d}\gamma + \tau_{t,0} \tag{1}$$

where $\tau_{t,0}$ is the eventual torque preload if $\gamma = 0$.

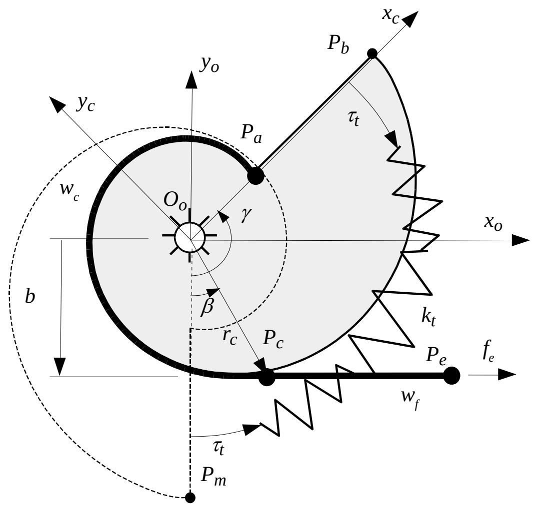

Fig. 10: LWWC-SEA: a non-linear spring obtained by a wire-wrapped cam.

The wire w is kept under tension by a force f applied to the free endpoint P_e. The so-far described mechanism is in static equilibrium if f is equilibrated by a reaction torque τ_t generated by k_t due to γ. The mechanism couples the translation of P_e parallel to f to a γ rotation of the cam.

Let us conveniently split γ in two components $\gamma = \gamma_b{}^o + \gamma_i{}^b$, where: a) $\gamma_b{}^o$ denotes the angular rotation of c from the condition $\gamma = 0$ to $P_t \equiv P_b$ and b) $\gamma_i{}^b$ denotes the rotation from $P_t \equiv P_b$ to P_t coincindent to the generic point Pi. The condition $\gamma_b \leq \gamma \leq \gamma_a$ guarantees that w_b is tangent to c and defines the actually exploitable range of motion of the mechanism.

Referring to Fig. 11, incerasing f, P_t slides from P_b to P_a as function of the length of the unwrapped segment of wire. Let us denote by $x_{e,\gamma}$ the horizontal displacement of P_e from a reference position, due to a γ angular displacement of c. Considering, as previously introduced, as reference condition, $P_t \equiv P_b$.

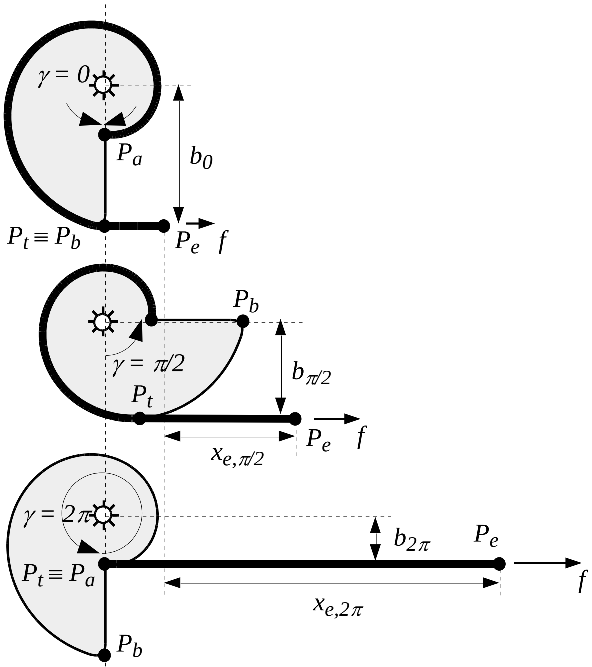

Fig. 11: Applying the force f to P_e, the wire is more and more unwrapped from c and P_t "slides" from P_b to P_a.

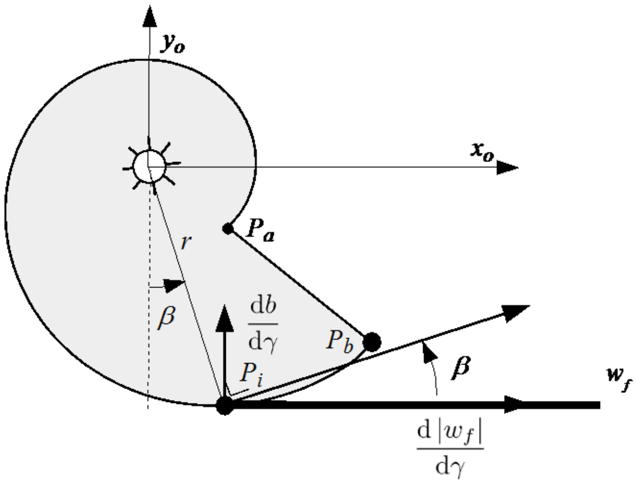

Fig. 12: Displacement of P_t.

Referring to Fig. 12 it is possible to evaluate the differential relation between the unwrapped wire and the cam rotation. It can be expressed as the component of the differential displacement of P_t tangentially to the cam profile, hence parallel to w_f. Let us conveniently denote the length of w_i by $|w_i|$.

$$\frac{\mathrm{d}\,|w_f|}{\mathrm{d}\gamma} = \left(\frac{\mathrm{d}P_t}{\mathrm{d}\gamma}\right)_t = r\cos\beta$$

Similarly, its normal component, i.e. the differential variation of b w.r.t. γ, can be evaluated.

$$\frac{\mathrm{d}b}{\mathrm{d}\gamma} = \left(\frac{\mathrm{d}P_t}{\mathrm{d}\gamma}\right)_n = r\sin\beta$$

It is possible to evaluate the wire unwrapping as function of the angular displacement γ by

$$|w_f| = \int \frac{\mathrm{d}\,|w_f|}{\mathrm{d}\gamma}\,\mathrm{d}\gamma \tag{2}$$

$$b = \int \frac{\mathrm{d}b}{\mathrm{d}\gamma}\,\mathrm{d}\gamma \tag{3}$$

Since the mechanism transforms the horizontal translation of P_f into a rotation of c, the torsional stiffness k_t results in the equivalent linear stiffness of P_e

$$k_l = \frac{k_t}{b^2} \tag{4}$$

Given the externally applied force f, the system is in quasi-static equilibrium if

$$\tau_t(\overline{\gamma}) = \overline{f}b(\overline{\gamma})$$

Both τ_t and b are function of γ and are obtained by (1) and (3), respectively.
The resulting linear displacement of P_e can be obtained by (2).
Therefore, a non-linear spring suitable to realize a variable-stiffness linear actuator can be obtained combining the stiffness of a torsional spring to a proper cam profile. Given the wide availability of (almost) linear off-the-shelf torsional springs, it is convenient, as previously introduced, to profile a cam as a spiral, leading to obtain an equivalent spring in P_e characterized by a monotonically increasing mechanical characteristic stiffness/displacement (i.e. if b increases as function of θ, k_l increases as function of $x_{e,y}$). This is convenient to guarantee a stable equilibrium of the VSA.

However, the configuration so-far considered has a unnegligible drawback: the direction of f has been considered constantly horizontal, while the vertical position of P_f changes as function of b, condition that occurs only if the length of w_f tends to infinity. In order to realize an equivalent linear spring performing a strict horizontal motion, it is convenient to refer to the scheme depicted in Fig. 13.

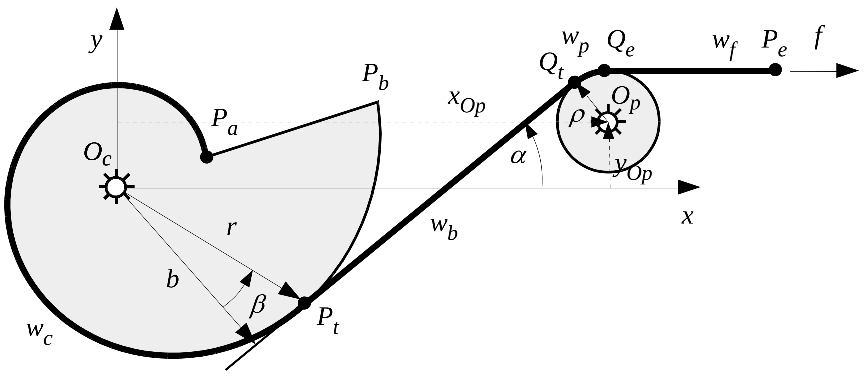

Fig. 13: The LWWC-SEA coupled with a pulley.

Referring to Fig. 13, let us consider that the wire w partially wraps c and, after detaching from it, is partially wrapped on a circular profile, namely p, representing a pulley, or any other mechanical constraint presenting a curvature radius. The wire w can be ideally split into four parts:

- w_c the part wrapped on c;
- w_b the part between c and p;
- w_p the part wrapped on p;
- w_f the remaining part up to the free endpoint P_e.

Let us define by following notable points:

- P_t the point in which w_b is tangent to c, between w_c and w_b;
- Q_t the point in which w_b is tangent to p, between w_b and w_p;
- Q_e the point in which w_f is tangent to p.

The angles α denotes the inclination of w_b w.r.t. x_o. In particular, α is determined by the line tangent to c and p passing through P_t.

The total length of the wire is therefore $w = w_c + w_b + w_p + w_f$.
The actual length of each segment of w is function of α. w_b lays on a line with a distance equal to b w.r.t. O_c, and a distance equal to ρ w.r.t. O_p. Referring to $\{o\}$, it is

$$P_t = (b \sin \alpha, -b \cos \alpha).$$

Considering that the line passing through a generic point $P = (x_P, y_P)$ with the angular coefficient $m = arctan(\varphi)$ is defined by

$$m(x - x_P) - (y - y_P) = 0$$

the line passing through P_c is defined by

$$\tan \alpha x - y - \frac{b}{\cos \alpha} = 0$$

Given a line expressed by $ax + by + c = 0$, the distance r from a point P is

$$r = \frac{ax_P + by_P + c}{\sqrt{a^2 + b^2}}$$

Therefore, from the previous equation it is possible to obtain the symbolic equation of α.
The intersection point between w_b and c and p respectively, are

$$P_t = (x_{Pt}, y_{Pt}) = (r \sin(\alpha + \beta), -r \cos(\alpha + \beta))$$

$$Q_t = (x_{Qt}, y_{Qt}) = (-\rho \sin(\alpha) + x_{Op}, \rho \cos(\alpha) + y_{Op})$$

The length of w_b is therefore

$$|w_b| = Q_t - P_t$$

3.2.1 The logaritmic spiral

The logarithmic spiral is defined, in polar coordinates, by [12]

$$r = ae^{b\theta}$$

with e being the base of natural logarithms, and a and b being arbitrary positive real constants. The rate of change of radius is:

$$\frac{\mathrm{d}r}{\mathrm{d}\theta} = abe^{b\theta} = br$$

The spiral has the property that the angle φ between the tangent and radial line at the point $P(r,\theta)$ is constant. This property can be expressed in differential geometric terms as

$$\beta = \arccos\left(\frac{rr'}{\|r\|\|r'\|}\right) = \arctan\frac{1}{b}$$

where $r' = \mathrm{d}r/\ \mathrm{d}\theta$.

From the point of view of an engineer or a designer it is important to use functional parameters, leading to define geometric parameters. Let us define the avarage stiffness variation, as

$$\Gamma k_l = k_l\,(s_a)/\,k_l\,(s_b)$$

where $k_l(s_a)$ and $k_l(s_b)$ denotes the wire stiffness if $s = 0$ and $s = s_M$, respectively.

In other words it is the ratio between the maximum and the minimum stiffness along the wire.

Considering, as previously introduced, a constant stiffness $k_{t,s}$ as function of θ, it is

$$\Gamma k_l = \frac{k_{t,s}}{b(s_0)\left(\frac{dx}{d\theta}\right)_{s_0}}\frac{b(s_M)\left(\frac{dx}{d\theta}\right)_{s_M}}{k_{t,s}} = \left(\frac{r(s_M)}{r(s_0)}\right)^2$$

leading to

$$\Gamma k_l = \left(\frac{e^{b\theta_M}}{e^{b\theta_0}}\right)^2 \Rightarrow b = \frac{\ln(\Gamma k_l)}{2\Delta\theta} \tag{5}$$

where $\Delta\theta$ is the total rotation of the cam. The a parameter is a scale factor of the logaritmic shape, defining the actual dimension of the cam. Given a maximum cam radius $r_M(\theta_M)$, considering a maximum rotation angle θ_M, it is

$$a = \frac{r_M}{e^{b\theta_M}}. \tag{6}$$

Therefore the use of a logaritmic spiral profile of the cam simplify its design phase.

3.3 Linear Wire-Wrapped Cam – Variable Stiffness Actuator (LWWC-VSA)

Referring to Fig. 7, it is possible to apply two antagonistic LWWC-SEA as depicted in Fig. 14.

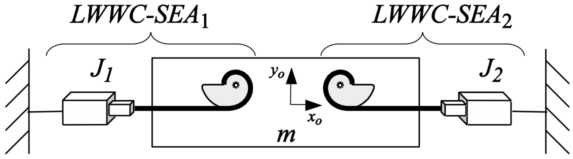

Fig. 14: The antagonistic *LWWC-SEA* feature the Variable Stiffness Actuator *LWWC-VSA*.

Referring to Fig. 15 let us denote by

$\delta = x_2 - x_1$ the distance between two reference points of wires

$\xi = x_m - x_h$ the displacement of the mobile part from the reference position,

where $x_h = (x_2 - x_1)/2$ is the equilibrium position of the mobile part.

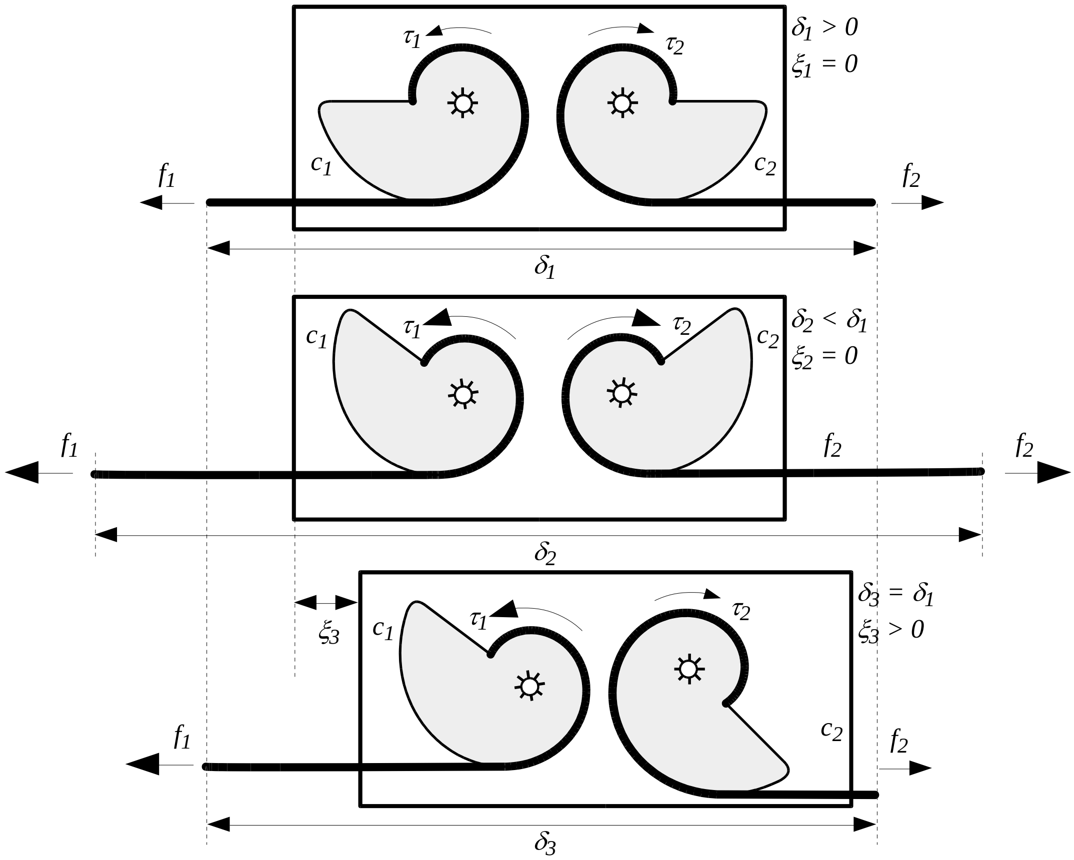

Fig. 15: Effect of modifying wire pretensioning and mobile body position.

The total force applied to the mobile part of the LWWC-VSA is

$$f_v = f_1 + f_2 \tag{7}$$

denoting by f_i the linear force applied to i-th LWWC-SEA.

Similarly, the resulting stiffness is

$$k_v = k_1 + k_2 \tag{8}$$

Both f_v and k_v are function of both δ and ξ.

4 Design

According to the actuation scheme illustrated in Fig. 14 and Fig. 15 the new version of LINarm (namely LINarm2) has been designed. The cam-based variable-stiffness actuation system is the heart of the new developed device.

4.1 Dimensioning

4.1.1 Actuation

The dimensioning phase of LINarm2 requires the definition of transmission and parameters in order to define geometrical parameters of custom made parts and choose commercial components. The dimensioning process takes as input technical specifications as the desired maximum/minimum stiffness (imposed according to experiences performed on LINarm1), joint torques/velocity and so on. Hereafter, a list of the main parameters of the cam-based transmission is reported. The section *spring* and *motor* refer to the selected spring and motor to be installed.

TRANSMISSION	
Min radius cam [mm]	**10**
Max radius cam [mm]	**33**
Max linear stiffness [N/mm]	**2**
Min linear stiffness [N/mm]	**0.2**
Radius wire pulley [mm]	**20**
Radius pulley encoder [mm]	**10**
Number holes encoder	**21**
Torsional stiffness @ min radius [Nmm/rad]	*200*
...[Nmm/°]	*3.490658504*
Torsional stiffness @ max radius [Nmm/rad]	*217.8*
...[Nmm/°]	*3.801327111*
SPRING	
Reference	*G.136.150.1275*
Ext. Diam. [mm]	*13.6*
Wire Diam. [mm]	*1.5*
Nr of Coils	*12.75*
Leg Position [°]	*270*
Free Len. [mm]	*20.625*
Leg Length [mm]	*54.4*
Dd [mm]	*8.3*
Spring Rate [N*mm/°]	*1.7593*
Material	*Stainless Steel*
Max M [N*mm]	*475*
Max F [daN]	*0.8731618*
Max angle [°]	*269.9*
Int. Diam. [mm]	*10.6*
Weight [g]	*8.184583*
Rotation	*Left rotation*
Tariff code	*4K*
Max Required Motor Torque [Nmm]	*950*
...[Nm]	*0.95*
MOTOR	https://www.pololu.c
Motor type	*Pololu 70:1 Metal Gearmotor 37Dx57L mm*
Max Torque [Nm]	**1.41**
rotational speed [rpm]	**150**
...[rad/s]	*15.70796327*
Max Torque Safety Ratio	*1.48*
Max stiffness safety Ratio	*1.008004649*
Max Velocity [mm/s]	*314.1592654*

4.1.2 The LWWC-SEA applied to LINarm2.

Considering dimensioning data reported in Section 4.1.1 the cam-based non-linear spring have been designed, its profile has been drawn and the mechanical characteristic of the actuator has been calculated. Taking into account the maximum stiffness variation and the maximum radius of the cam, it was possible to evaluate the logaritmic profile of the cam applying (5) and (6).

Considering:

$$\Gamma k_l = k_l\,(s_a)/\,k_l\,(s_b) = 10$$

$$\Delta\theta = 2\pi$$

$$r_b = 0.034\text{m (maximum radius of the cam)}$$

it results

$$a = 0.01075\text{m}$$

$$b = 0.1832$$

In Fig. 16 the frontal view of the mobile body of LINarm is illustrated with its main dimensions.

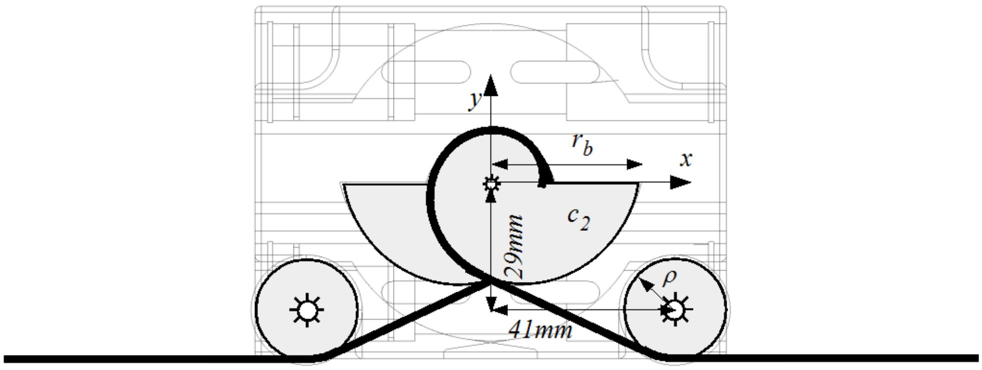

Fig. 16: Frontal view of the mobile body of LINarm2.

Given the actual dimensions of the prototype, a simulation of the wire unwrapping is reported in Fig. 17.

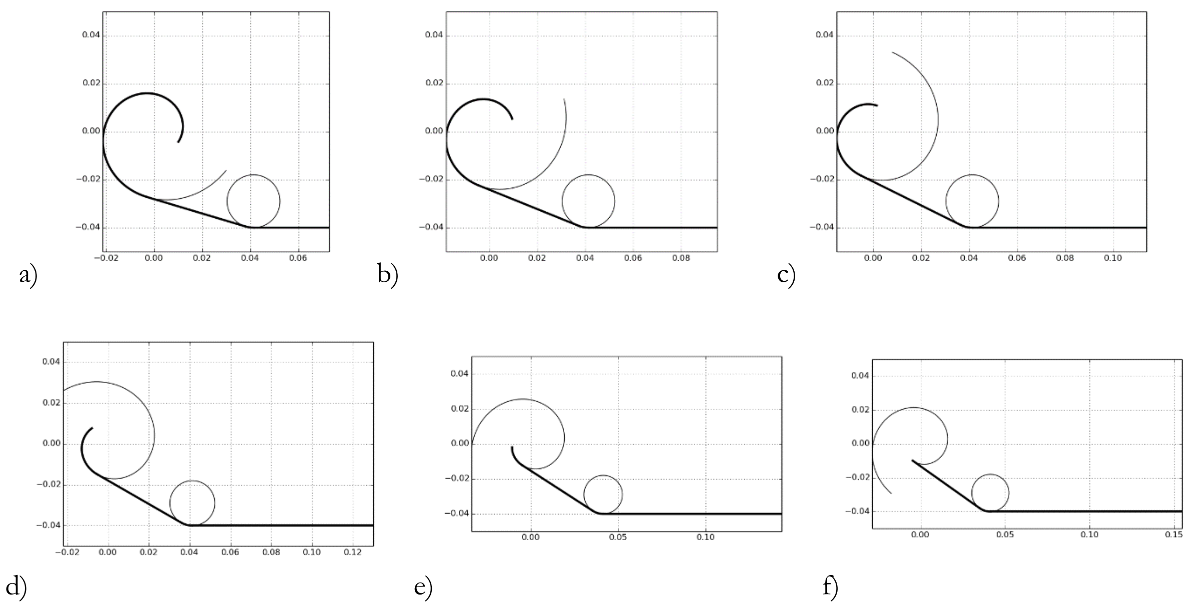

Fig. 17: Kinematic simulation of wire-unwrapping, from a) to f).

The characteristic curves of the LWWC-SEA are reported hereafter.

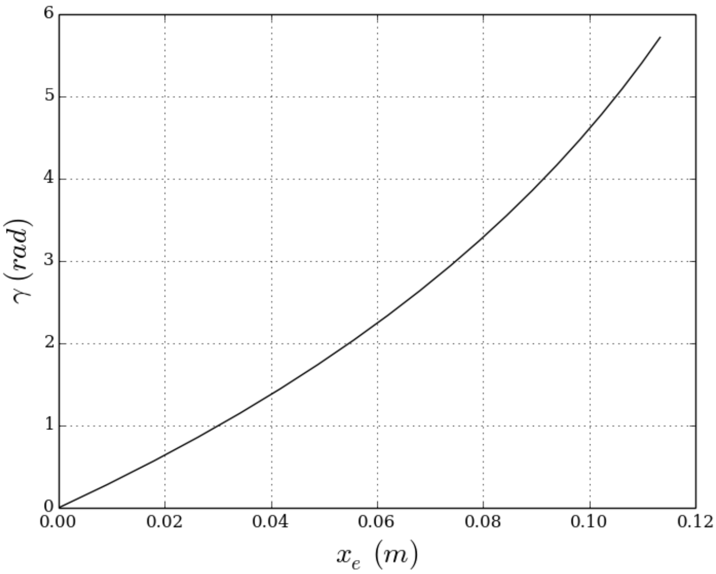

Fig. 18: Rotation of the cam γ as function of the length of the unwrapped wire x_e.
Note: the curve is not a line because of the presence of the pulley.

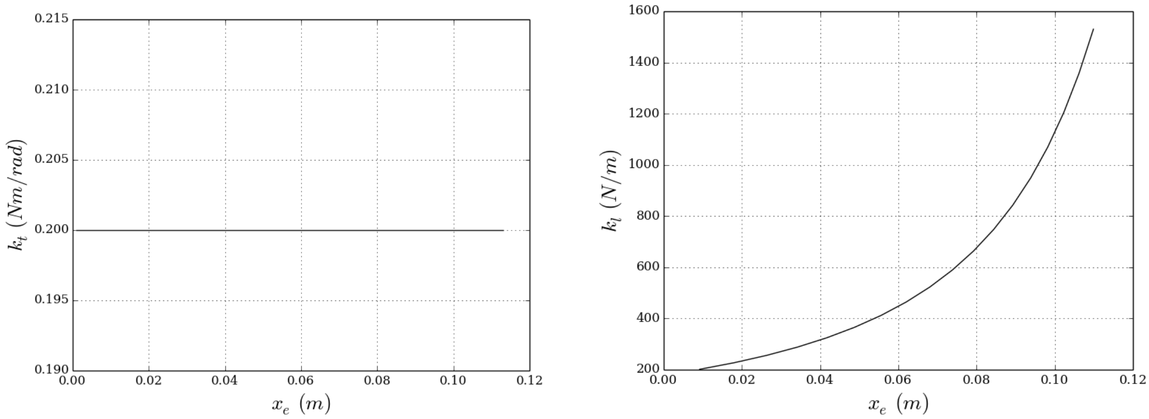

Fig. 19: Torsional stiffness of the selected commercial spring (left) and linear stiffness of the wire wrapped on the cam (right), as function of the length of the unwrapped wire. The stiffness non-linearity, required to realize a VSA, is notable.

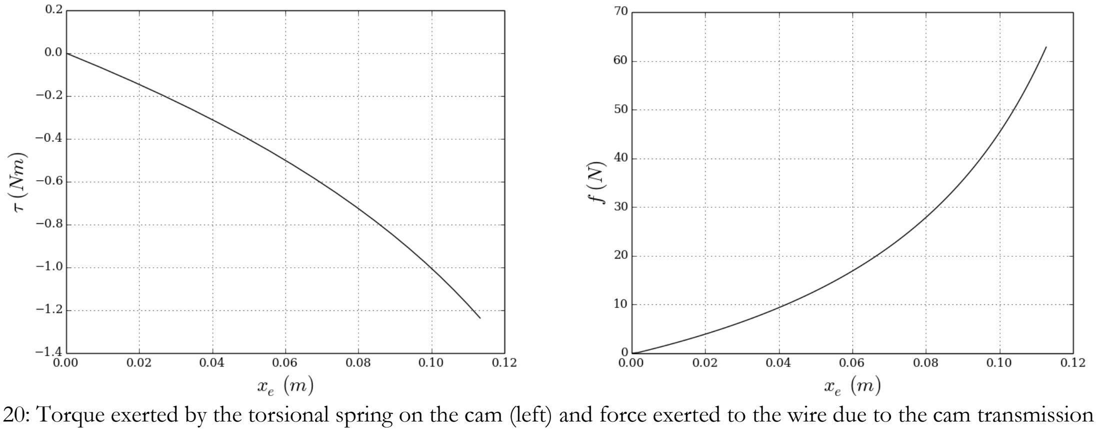

Fig. 20: Torque exerted by the torsional spring on the cam (left) and force exerted to the wire due to the cam transmission (right), as function of the length of the unwrapped wire.

4.1.3 The LWWC-VSA applied to LINarm2.

The force and the stiffness of the LWWC-VSA as function of δ and ξ (Section 3.3) have been evaluated applying (7) and (8). These surfaces will be implemented in the control system to tune in real-time forces and stiffness of the mechanical device (Chapter 5).

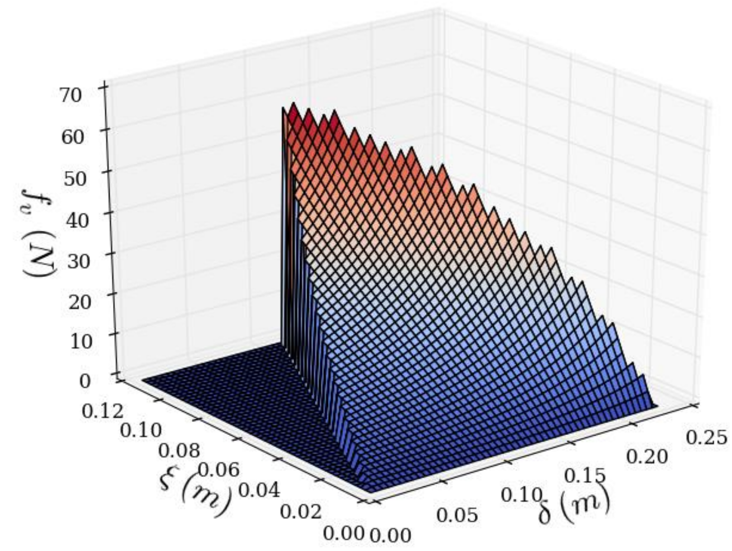

Fig. 21: Force on the mobile body as function of δ and ξ.

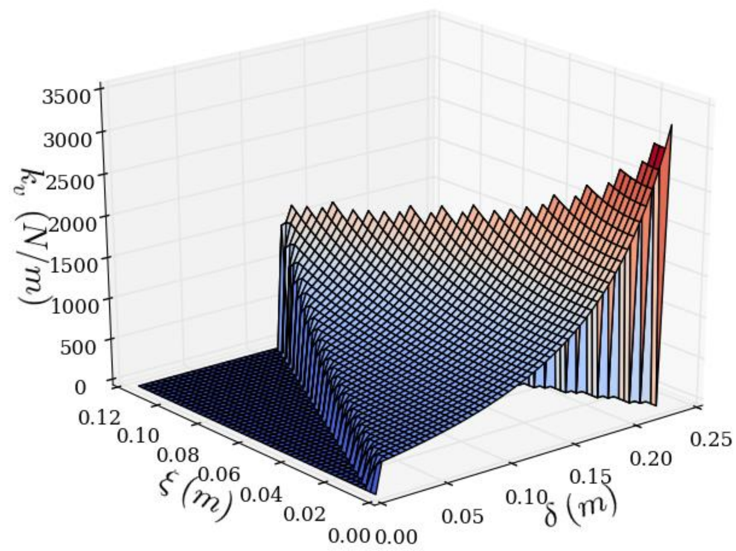

Fig. 22: Stiffness of the mobile body as function of δ and ξ.

4.2 Detailed design

In this section the detailed mechanical design of LINarm2 is reported. The global assembly and main subassemblies are reported with indications of the main parts constituting the device.

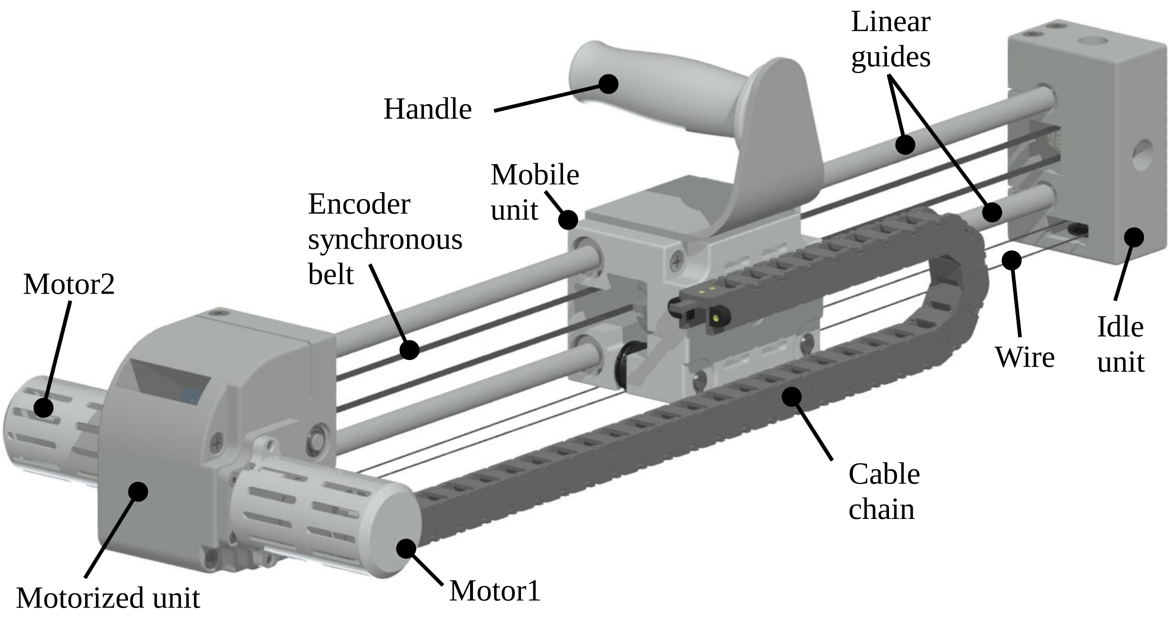

Fig. 23: Assembled view of LINarm2.

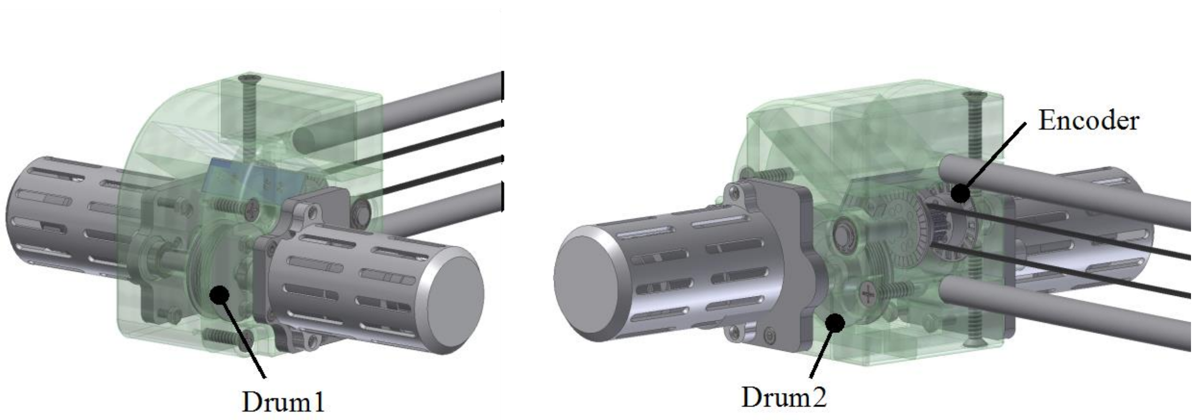

Fig. 24: Assembled view of the motorized unit. Drums wraps wires and are constrained to motors to control wire elongations. Each motor embeds an incremental encoder. An third encoder is used to measure the position of the mobile unit.

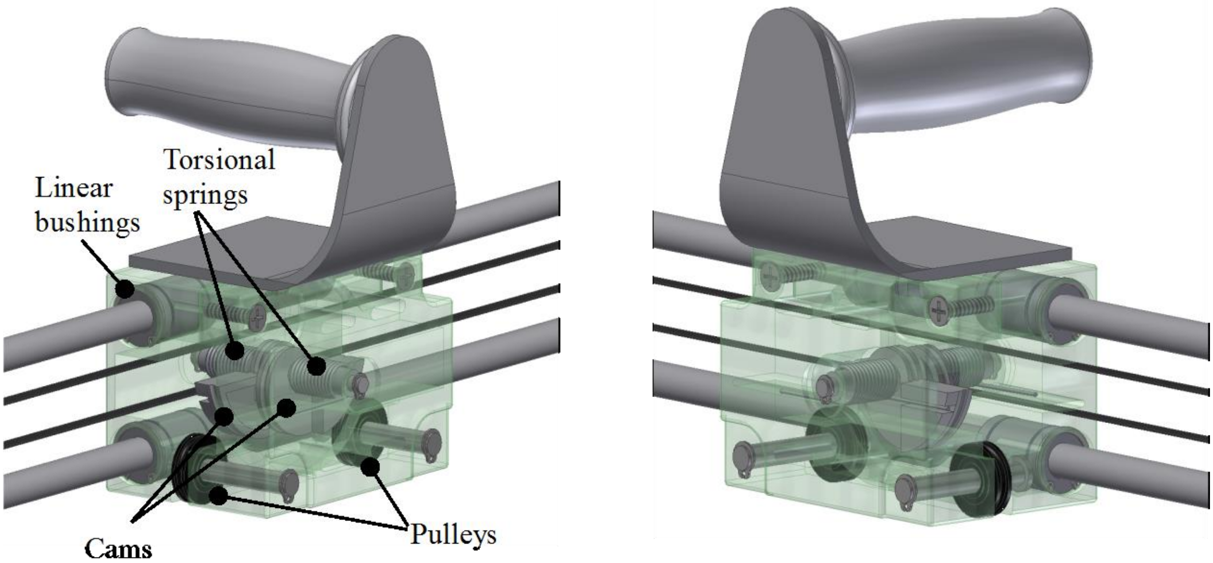

Fig. 25: Assembled view of the mobile unit. A single shaft supports the cams of the LWWC-VSA.

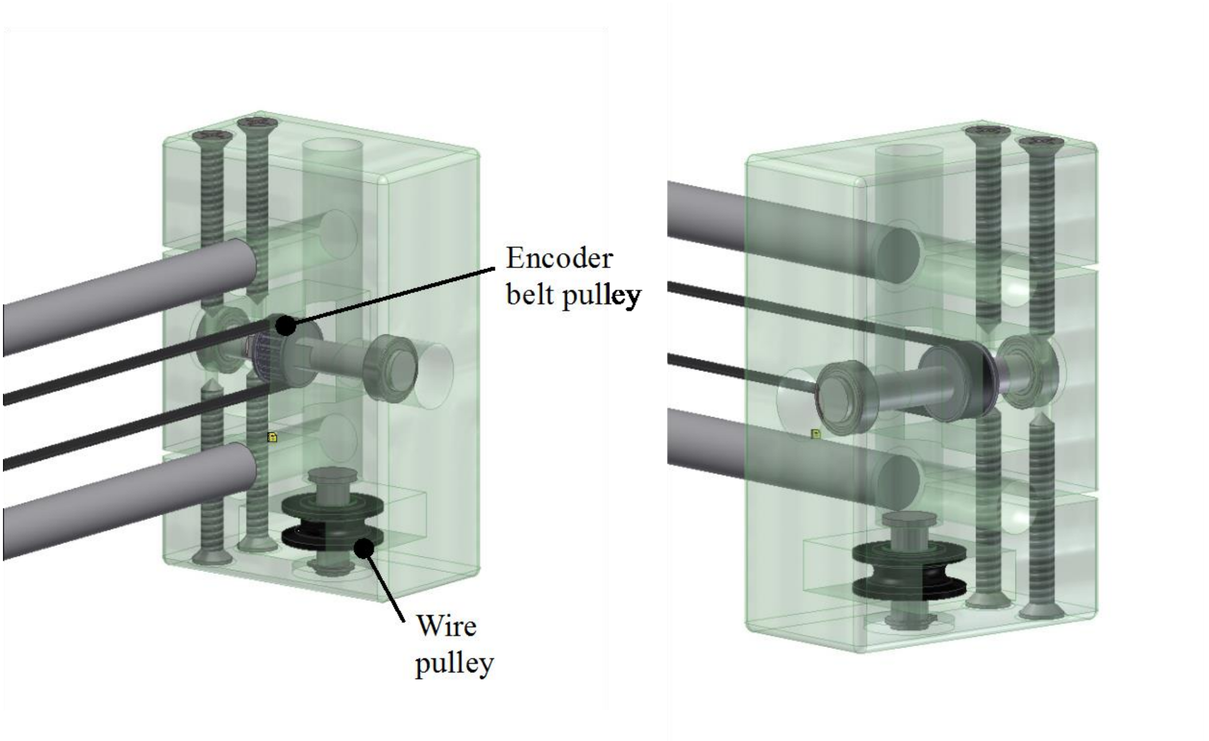

Fig. 26: Assembled view of the idle unit. It constraints the linear guides, and contains the idle pulleys of the wire and of the encoder synchronous belt.

4.3 Covering

In order to fulfill regulations and, in particular, IEC 60601-1-11:2010 and all norms referred by it, it is necessary to design a structure protecting the mechanism and its mobile parts.
A smooth and rounded design has been proposed as the main shape for the shell, in order to guarantee a safe and good-looking product without any sharp edge which could be dangerous for patients or clinical staff. The rounded shape will also guarantee an easy to clean surface, resulting in a more appropriate device for clinical and health purposes. The structure is based on two symmetrical shells which have to be respectively mounted on the left and on the right side of the device. In order to guarantee the correct manufacturing of the structure, each shell is formed by two pieces: a big one which is intended to cover the main portion of the device and a small one, which is the cover for the electric motor. Prior to be mounted onto the device, these two pieces have to be assembled together.
The LINarm device is designed to be low-cost and produced in a limited number of copies per year. To maintain this philosophy a correct manufacturing strategy has to be performed. Two possible solutions have been found: the first one is vacuum-forming, the second one is composite material lamination.
Both solutions are compatible with the proposed shape and will result in a solid but lightweight structure capable of resisting to several impacts and preventing the insertion of hands or other parts of the body into the mechanism.
In the case of vacuum-forming, PVC sheets will be used. This manufacturing solution will guarantee an out-of-the-mould shell with a smooth and high-glossy finish without the need of any additional process. In order to produce each of the two shells, an aluminium mould with the cost of around 5000 € will be needed.
In the case of composite material lamination, fiberglass sheets will be used in addition to polyester resin. Fiberglass artefacts could be very strong, but they cannot be very smooth and good-looking unless the use of a layer of gelcoat, which will guarantee a high-glossy finish to the product. Even in the case of composite lamination, a mould with a cost in the order of hundreds of Euros will be needed to produce every of the two shells. In this case a fiberglass mould could be used, in order to reduce costs compared to the previous case. Anyway in the case of fiberglass lamination it has to be kept in mind that the material cost is higher than the vacuum-forming solution with PVC.
Each of the two purposed solution is compatible with the design of the device and with its philosophy and in both cases shells could be polished or painted in order to obtain a glossy and good-looking surface and to accomplish every aesthetic need.

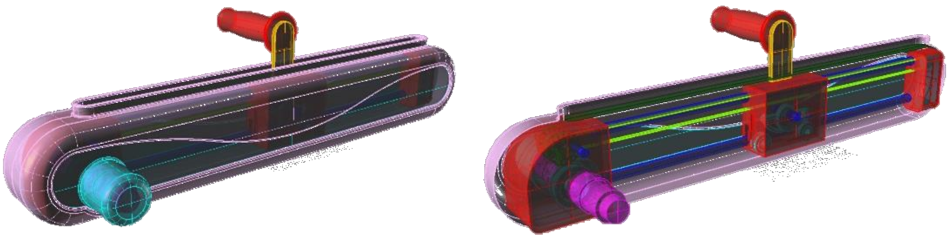

Fig. 27: Assembled and open view of the LINarm2 covering.

Fig. 28: Rendered views of alternative covering solutions.

4.4 Scenarios

The linear actuation module described in previous sections will be supported by a commercial spherical joint (Manfrotto MH057M0), enabling it to be oriented along different directions allowing the execution of reaching movements along different inclinations (Fig. 29), hand-to-mouth movements and also movements along other directions (e.g. lateral movement with the direction of movement normal to the sagittal plane, Fig. 30).

In order to satisfy desired functional requirements (Chapter 2.1) the following solutions will be realized.

1) integrate in the device a support able to fix the spherical joint to a table, enabling the possibility to incline vertically and horizontally the movement direction of LINarm2;
2) to foresee a proper flange to mount the spherical joint on an external support (e.g. a tripod).

The first solution will guarantee the possibility to fix LINarm to the table. This type of support will allow the execution of frontal (and eventually also lateral) reaching with different inclinations (similarly to the Tailwind device). It will not allow the possibility to perform HtMM.
The second solution will allow the execution of more movements including the HtMM.

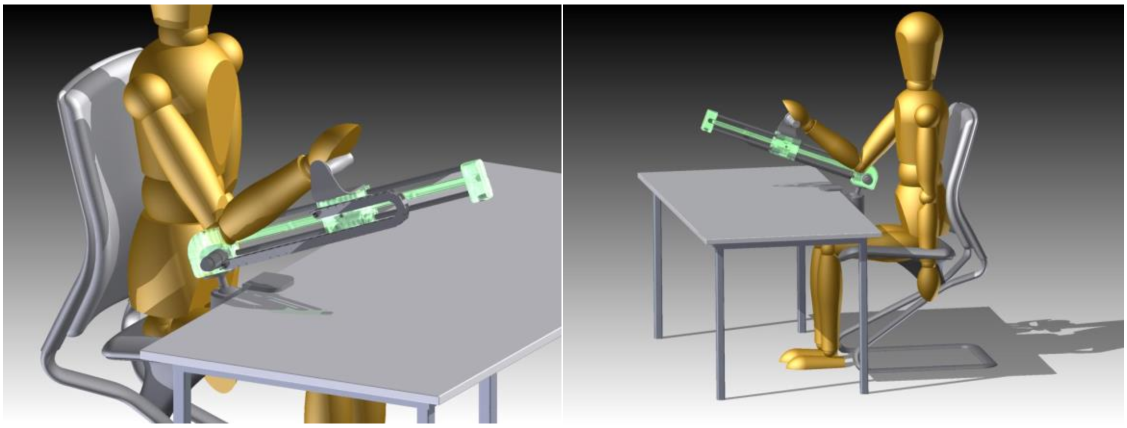

Fig. 29: LINarm2 installed on a table oriented to perform reaching movements.

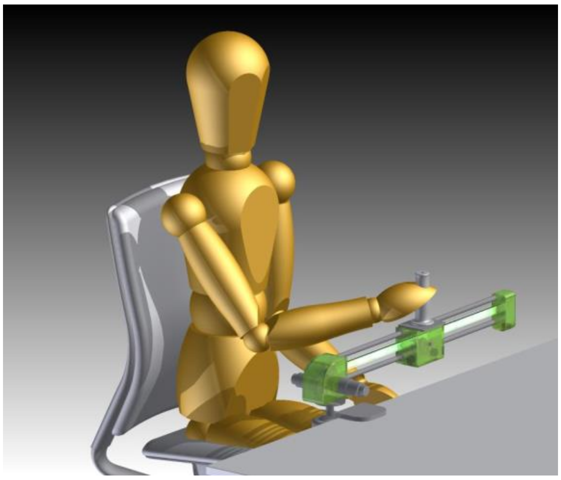

Fig. 30: LINarm2 installed on a table oriented to perform lateral movements.

5 Control and Electronics

A simplified representation of the LINarm2 mechatronic system is represented in Fig. 31. The control system is in charge of controlling in real time both the equilibrium position x_e and the stiffness k_q of the device, controlling the actuators positions q_1 and q_2.

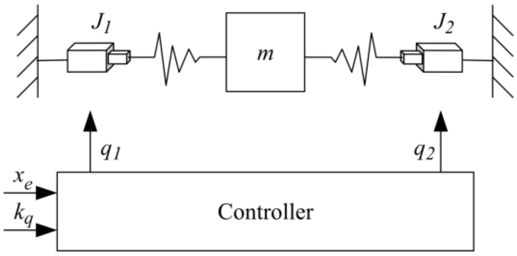

Fig. 31: The position of the end-effector equilibrium point and its stiffness are defined controlling in position the two actuators.

The final design of the prototype (Fig. 1) is characterized by two cheap rotational motors (Pololu Metal Gearmotor 37Dx57L mm) equipped by an internal incremental rotary encoder.
The electrical layout and connections are represented in Fig. 32. The control system is implemented in an Arduino-Due microcontroller board, in charge of closing control loops in real time and controlling motors through the Pololu Dual VNH5019 Motor Driver Shield. The control system is implemented exploiting the open-source ChibioOS/RT Real-Time Operating System, compiled for the ARM Cortex-M3 CPU. A A20-OLinuXino-MICRO, a low-cost and compact ARM-based computer, interfaced to the Arduino board through a serial connection, is in charge of high-level functionalities control, therapeutic exercises programming and rendering of an engaging virtual environment.
Refer to *Deliverable D2.1 - Control system architecture and components* for details.

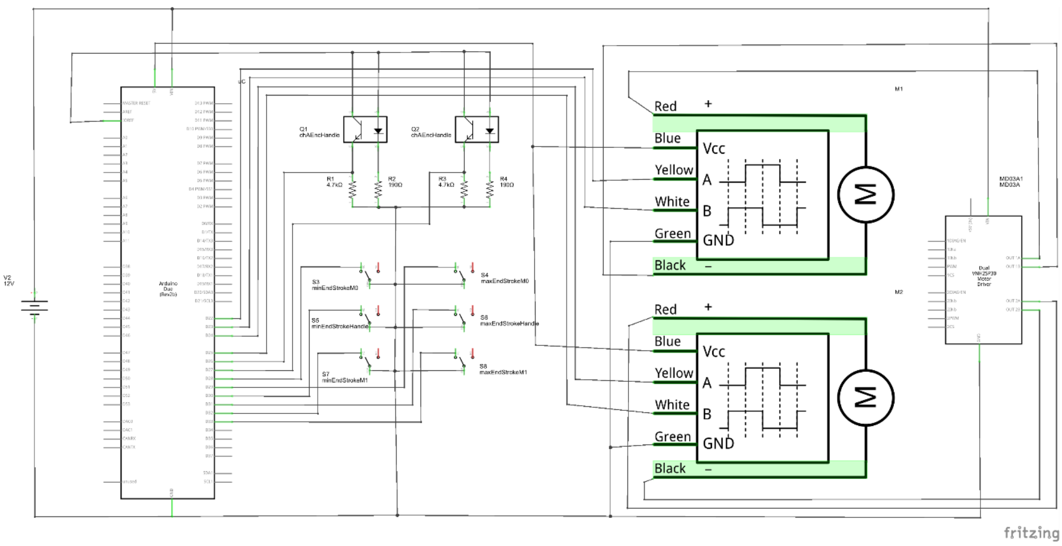

Fig. 32: Electrical components and connections.

References

[1]. Rau G, Disselhorst-Klug C, Schmidt R. Movement biomechanics goes upwards: from the leg to the arm. *J Biomech.* 2000 Oct;33(10):1207-16.

[2]. M. Caimmi, S. Carda, C. Giovanzana, E. S. Maini, A. M. Sabatini, N. Smania, and F. Molteni. Using kinematic analysis to evaluate constraint-induced movement therapy in chronic stroke patients. *Neurorehabilitation and neural repair*, 22(1):31–39, 2008.

[3]. M Caimmi, E Guanziroli, M Malosio, Nicola Pedrocchi, Federico Vicentini, Lorenzo Molinari Tosatti, F Molteni. Normative Data for an Instrumental Assessment of the Upper-Limb Functionality. Article ID 484131 *Biomed Res. Int.* In Press.

[4]. M. Caimmi, A. Chiavenna, F. Digiacomo, G. Gasperini, C. Giovanzana, M. Malosio, N. Pedrocchi, A. Scano, F. Vicentini, F. Molteni, e L. Molinari Tosatti, Successfully use a passive approach in upper-limb robotic rehabilitation of chronic stroke patients. *1st Clinical Movement Analysis World Conference*, 29 September – 4 October 2014, Rome, Italy Gait and posture 2015. In press.

[5]. Pang MY, Harris JE, Eng JJ.A community-based upper-extremity group exercise program improves motor function and performance of functional activities in chronic stroke: a randomized controlled trial. *Arch Phys Med Rehabil* 2006:87:1-9.

[6]. Schweighofer N , Choi Y, Winstein C, Gordon J. Task-oriented rehabilitation robotics. *Am J Phys Med Rehabil.* 2012 Nov;91(11 Suppl 3):S270-9.

[7]. M. Malosio, M. Caimmi, G. Legnani, and L. Tosatti, “Linarm: a low-cost variable stiffness device for upper-limb rehabilitation,” in *Intelligent Robots and Systems (IROS 2014), 2014 IEEE/RSJ International Conference on*, pp. 3598–3603, Sept 2014.

[8]. B. Vanderborght, A. Albu-Schaeffer, A. Bicchi, E. Burdet, D. G. Caldwell, R. Carloni, M. Catalano, O. Eiberger, W. Friedl, G. Ganesh, M. Garabini, M. Grebenstein, G. Grioli, S. Haddadin, H. Hoppner, A. Jafari, M. Laffranchi, D. Lefeber, F. Petit, S. Stramigioli, N. Tsagarakis, M. Van Damme, R. Van Ham, L. C. Visser, and S. Wolf, “Variable impedance actuators: A review,” *Robot. Auton. Syst.*, vol. 61, pp. 1601–1614, Dec. 2013.

[9]. K.-H. Nam, B.-S. Kim, and J.-B. Song, “Compliant actuation of parallel-type variable stiffness actuator based on antagonistic actuation,” *Journal of Mechanical Science and Technology*, vol. 24, no. 11, pp. 2315–2321, 2010.

[10]. Wikipedia, “Arc length — wikipedia, l’enciclopedia libera,” 2015. [Online; verified on August 10th, 2015].

[11]. C. Stover and E. W. Weisstein, “’polar coordinates.’ from mathworld–a wolfram web resource..”

[12]. “Weisstein, eric w. ”logarithmic spiral.” from mathworld–a wolfram web resource..” url http://mathworld.wolfram.com/LogarithmicSpiral.html.